An Electrochemical Impedance Spectroscopic Study of the Electronic and Ionic Transport Properties of Spinel $LiMn_2O_4$

Quan-Chao Zhuang,*,† Tao Wei,† Li-Li Du,† Yong-Li Cui,† Liang Fang,† and Shi-Gang Sun*,‡

School of Materials Science and Engineering, China University of Mining and Technology, Xuzhou 221116, China, and State Key Lab of Physical Chemistry of Solid Surfaces, Department of Chemistry, College of Chemistry and Chemical Engineering, Xiamen University, Xiamen 361005, China

Received: November 17, 2009; Revised Manuscript Received: March 12, 2010

Electrochemical impedance spectra (EIS) for lithium ion insertion and deinsertion in spinel $LiMn_2O_4$ were obtained at different potentials and different temperatures during initial charge−discharge cycle. The results revealed that, at intermediate degrees of intercalation, three semicircles appeared in the Nyquist diagram. This new phenomenon has been investigated through EIS measurements as a function of temperature. It has found that the high frequency semicircle and the middle to high frequency semicircle begin to overlap each other above 20 °C, which indicates that the high frequency compressed semicircle commonly obtained at room temperature in the literature may consist of two semicircles. This signifies that the effects of the electronic and ionic transport properties of lithium intercalation materials clearly appear as separate features in the EIS spectra at low temperatures. A new equivalent circuit that includes elements related to the electronic and ionic transport, in addition to the charge transfer process, is proposed to simulate the experimental EIS data. The change of kinetic parameters for lithium ion insertion and deinsertion in spinel $LiMn_2O_4$ as a function of potential in the first charge−discharge cycle is discussed in detail, and a modified model is proposed to explain the impedance response of the insertion materials for lithium ion batteries.

1. Introduction

Rechargeable lithium ion batteries have been used in a wide variety of portable electric devices owing to their high energy densities. However, these batteries still need to be improved before they can be used in hybrid electric vehicles (HEVs).[1,2] Rapid charge−discharge and high-temperature properties are required for lithium ion batteries to be used for high power applications. Spinel $LiMn_2O_4$ is at present a very good candidate as a cathode material for lithium ion batteries because of its high theoretical energy density, high natural abundance, low cost, acceptable environmental characteristics, and good safety properties.[3−6] Therefore, battery systems based on the $LiMn_2O_4$/carbon couple have been used commercially in many types of electronic equipment.[7] However, their power density is generally low because of a large polarization at high charge−discharge rates.[8−11] To overcome these problems, it is necessary to understand the kinetics of the lithium ion insertion−deinsertion process in the spinels since they govern the intercalation−deintercalation rate and would undoubtedly facilitate further electrode optimization. It would be desirable to see what kinetics and other relevant properties such as charge transfer resistance, diffusion, material resistance, electronic resistance, etc. are changed in new materials in a way that is independent of particular electrode composition or the electrolyte used.

Electrochemical impedance spectroscopy, or EIS, is a commonly used technique to analyze electrochemical processes occurring at electrode/electrolyte interfaces, and has been widely used for the studies of electrochemical lithium intercalation into carbonaceous materials and transition metal oxides.[12−30] Lithium insertion results from a series of complex phenomena including lithium ion diffusion in the electrolyte, migration through the surface passivation film (also called the solid electrolyte interphase film, abbreviated as SEI film) covered on the electrode, charge transfer through the electrode/electrolyte interface, and diffusion in the bulk of active mass that is often described as finite space or restricted diffusion, etc. Thanks to the differences in their time constants, EIS is a suitable technique for these investigations and can allow us to separate most of these phenomena.

In this study, the processes of the first delithiation/lithiation of the spinel $LiMn_2O_4$ electrode were investigated by EIS. A new phenomenon that has never been reported before is described, namely that at intermediate degrees of intercalation the effects of the electronic and ionic transport properties of lithium intercalation materials appear as separate features in the spectra at lower temperatures. Accordingly, a modified model is proposed to explain the impedance response of the insertion materials of lithium ion batteries. The inclusion in the new equivalent circuit of an element related to the electronic conductivity results in a more realistic picture of the physical phenomena occurring during the lithium intercalation/deintercalation process. Special emphasis is placed on the ionic and electronic transport properties of the spinel $LiMn_2O_4$ electrode in the first delithiation−lithiation process.

2. Experimental Methods

All electrochemical impedance measurements were conducted in a three-electrode glass cell with Li foils as auxiliary and reference electrodes. The spinel $LiMn_2O_4$ electrodes used in this study were prepared by spreading a mixture comprising, by weight, 80% commercially available spinel $LiMn_2O_4$ (provided

* To whom correspondence should be addressed. Tel.: +86 516 83591877. Fax: +86 516 83591870. E-mail address: zhuangquanchao@126.com; sgsun@xmu.edu.cn.
† China University of Mining and Technology.
‡ Xiamen University.

10.1021/jp9109157
Published on Web 04/19/2010

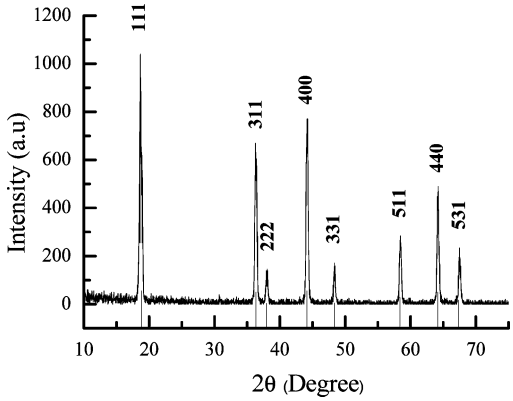

Figure 1. JCPDS standard of spinel $LiMn_2O_4$ and XRD patterns of commercial $LiMn_2O_4$.

by Amperex Technology Limited Co., Dongguan, China), 2% acetylene black, 13% mesocarbon microbeads (Shanshan Co., Shanghai, China), and 5% polyvinylidene fluoride (PVdF, Kynar FLEX 2801, Elf-atochem, USA) binder dissolved in *N*-methyl-2-pyrrolidone (Fluka, Inc.) onto an aluminum foil current collector. The electrode film thus obtained was dried at 120 °C for 12 h under vacuum prior to use. Charge−discharge cycles were carried out at 0.1 C in a 2025 coin cell using lithium metal as the second electrode, over a potential range between 3.5 and 4.3 V. The electrolyte was 1 mol·L^{-1} $LiPF_6$−EC:DMC (volume ratio, 1:1, Guotaihuarong Co., Zhangjiagang, China).

The phase identification was carried out by powder XRD using Cu Kα radiation on a Rigaku D/Max-3B diffractometer. Diffraction data were collected by step scanning over an angular range of 10−75° with a step width of 0.02° (35 KV, 30 mA). The particle morphologies of the samples were examined with a scanning electron microscope (SEM, Hitachi, S-3000N).

3. Results and Discussion

The joint committee for powder diffraction studies (JCPDS) of spinel $LiMn_2O_4$ and XRD patterns of commercial $LiMn_2O_4$ is shown in Figure 1. All patterns are in good agreement with the JCPDS standard, and all the diffraction peaks could be indexed to the cubic spinel structure with the space group *Fd*3*m*. Figure 2 shows typical SEM micrographs of the commercial $LiMn_2O_4$. It can be seen that the electrode active mass has nearly cubic morphology and comprises two types of particles agglomerated together, namely, particles with a diameter of 2−3 μm and particles with a diameter of 7−9 μm.

Figure 3 illustrates the first 10 charge−discharge curves of Li/$LiMn_2O_4$ cells (Figure 3a) and the variations in the discharge capacity of spinel $LiMn_2O_4$ with cycle number (Figure 3b). It can clearly be seen that the charge/discharge curves of the samples have two voltage plateaus at approximately 4.0 and 4.1 V, which is a typical feature of the spinel $LiMn_2O_4$. The two voltage plateaus specify that the insertion and extraction of lithium ions occur in two stages. The first voltage plateau, at about 4.0 V, is attributed to the removal of lithium ions from half of the tetrahedral sites in which Li−Li interactions occur. The second voltage plateau observed at about 4.1 V is due to the removal of lithium ions from the other tetrahedral sites, in which lithium ions do not have Li−Li interactions.[31] The initial specific discharge capacity of the spinel $LiMn_2O_4$ is close to 110 mAh·g^{-1}, yet after over 100 cycles the capacity retention of the spinel $LiMn_2O_4$ is still above 90%, indicating an excellent electrochemical performance.

To investigate the lithium ion insertion mechanism at the electrode/electrolyte interface, EIS measurements were carried

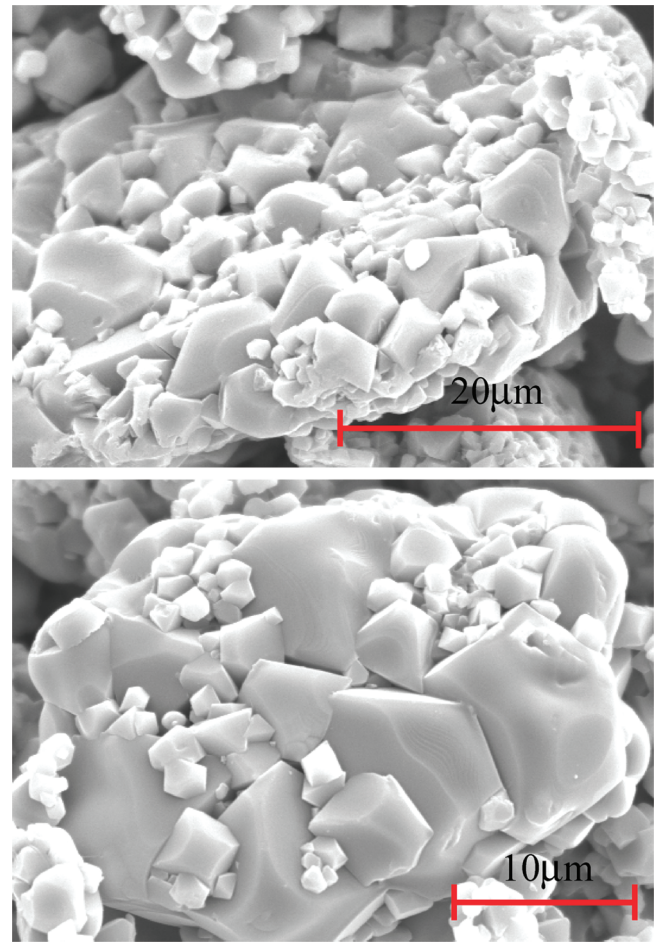

Figure 2. SEM images of commercial spinel $LiMn_2O_4$.

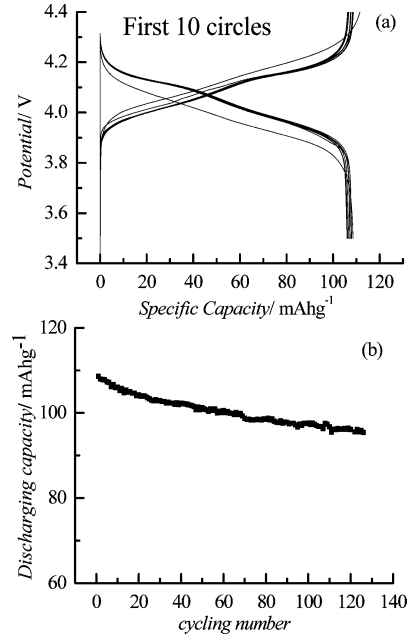

Figure 3. (a) Charge−discharge curves of Li/$LiMn_2O_4$ cells. (b) Variations in the discharge capacity with cycle numbers.

out for the $LiMn_2O_4$ electrode during the first charge−discharge cycle in 1 mol·L^{-1} $LiPF_6$−EC:DMC electrolyte at about 10 °C. Figure 4 and Figure 5 show the Nyquist plots obtained from the spinel $LiMn_2O_4$ electrode in the potential region from 3.5 to 4.3 V during the first charge−discharge cycle. The plots show an atypical trend for compounds of the spinel family, as can be

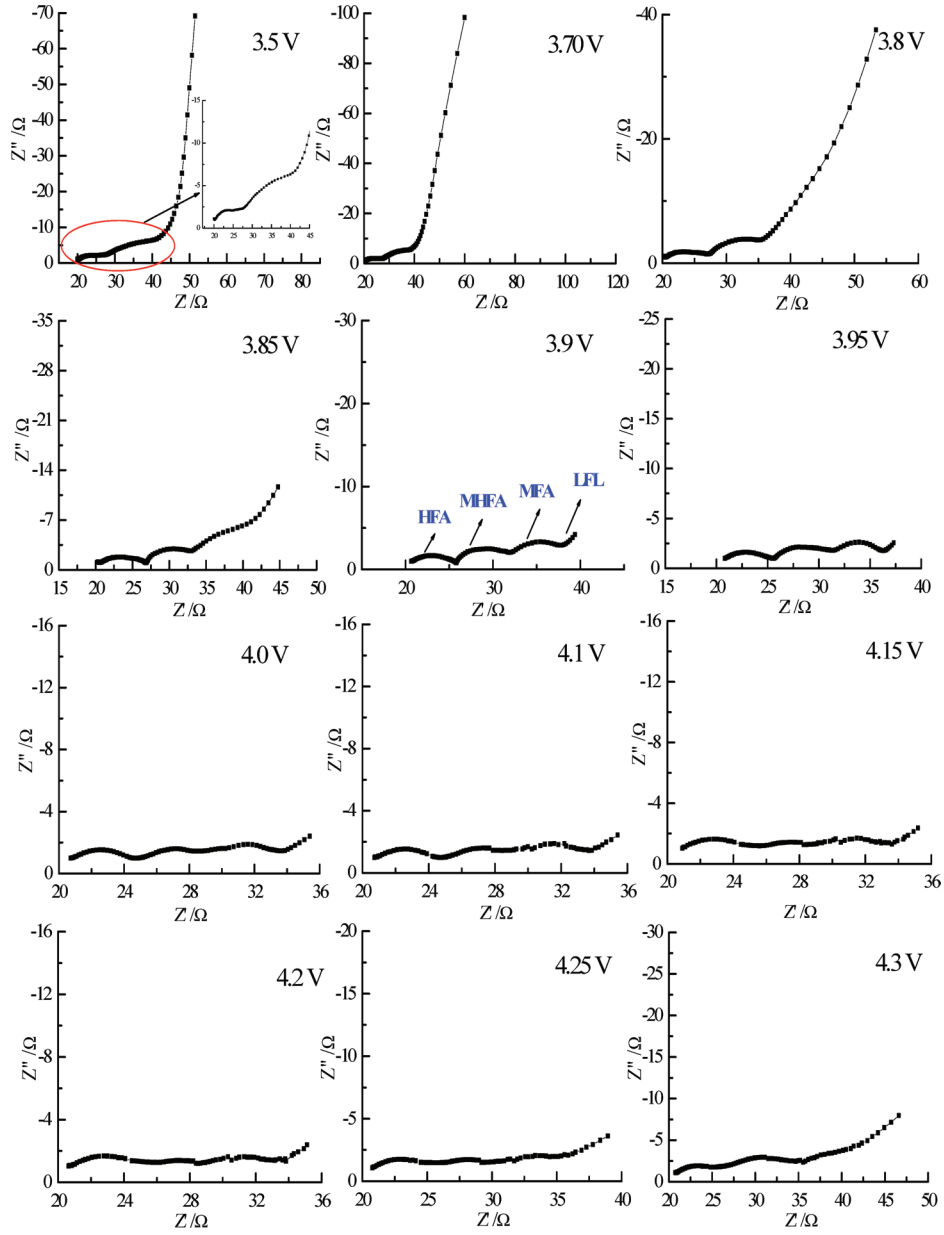

Figure 4. Nyquist plots of the spinel $LiMn_2O_4$ electrode at various potentials from 3.5 to 4.3 V during the first delithiation at 10 °C.

seen from the plots in Figure 4. As well as a high frequency semicircle (HFS) and an inclined line, a new semicircle in the middle to high frequency (MHFS) clearly emerged at a potential between 3.5 and 3.7 V. Along with increasing the polarization potential, the HFS and MHFS did not change significantly, while the inclined line, which is strongly potential dependent, shows an increasing tendency to move toward the real axis; and at last, another semicircle (middle frequency semicircle, abbreviated as MFS) and a steep sloping line (here called LFL in short) are formed in the low frequency region. At intermediate degrees of intercalation, 3.9 V for example, the Nyquist plot clearly consists of four parts, essentially three semicircles and one line. To our knowledge, this unique phenomenon has never been reported before in the literature. It is known from the literature that most researchers[28−35] do not see three semicircles but three parts, namely, a semicircle in the high frequency region, another semicircle in the middle frequency region, and a Warburg-type element in the low frequency region at intermediate degrees of intercalation, but without the MHFS. According to Aurbach and his co-workers,[28,29,35] the high frequency semicircle is related to lithium ion migration through the SEI film covered on the spinel $Li_xMn_2O_4$, the middle frequency semicircle is attributed to charge-transfer through the electrode/electrolyte interface, and the low frequency line is assigned to solid state diffusion of the lithium ion in the $Li_xMn_2O_4$ matrix.

This new phenomenon observed in the present paper puts forward two new questions. First, why has the MHFS appeared in this measurement? And second, what should be the origin of the MHFS?

To investigate further the experimental phenomenon described above, the effect of temperature has been taken into consideration. Additional EIS measurements for the $LiMn_2O_4$ electrode were carried out during the first delithiation phase under the same conditions as above, except for the temperature. The impedance spectra (10^5-10^{-2} Hz, 5 mV perturbation) were recorded at nine different temperatures from −10 to 30 °C. The experimental procedures were as follows. First, the potential of the electrode was slowly polarized to the required value (3.9 and 3.98 V) at room temperature, and then the temperature was

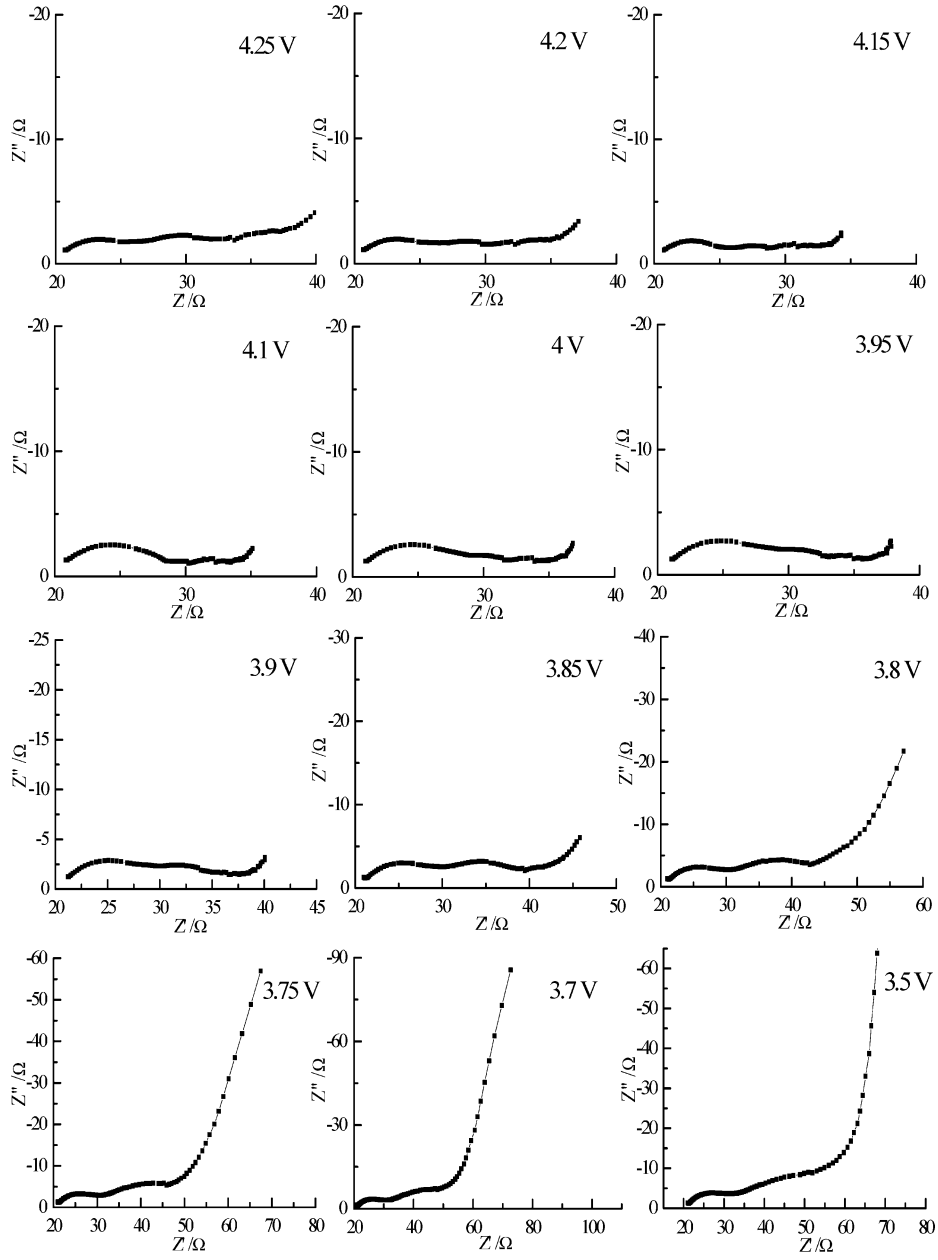

Figure 5. Nyquist plots of the spinel $LiMn_2O_4$ electrode at various potentials from 4.3 to 3.5 V during the first lithiation at 10 °C.

reduced to 10 degrees below zero using a temperature controller, where it was kept for 1 h so that the system was stable. Afterward, EIS measurements were taken at the former temperature, then at 5 degree increments at 3.90 and 3.98 V until 30 degrees above zero (allowing a sufficient equilibration time after each temperature variation).

Figure 6 displays a sequence of characteristic Nyquist plots recorded at constant potential but at various temperatures. For the sake of clarity, each plot is shifted by 5 Ω along the imaginary axis. In general, as shown in Figure 6, the absolute impedance decreases significantly with increasing temperature. The Nyquist plots consisted of three semicircles below the freezing point, namely, the HFS, MHFS, and MFS, while the LFL appeared above 0 degrees. As the temperature increased, it is interesting to observe that the MFS and the MHFS begin to overlap each other, and when the temperature reached 15 °C, the MFS and the MHFS were totally merged into one single compressed semicircle, exhibiting that the temperature clearly enhances the separation of two different physical phenomena by affecting them in a different way by virtue of having different

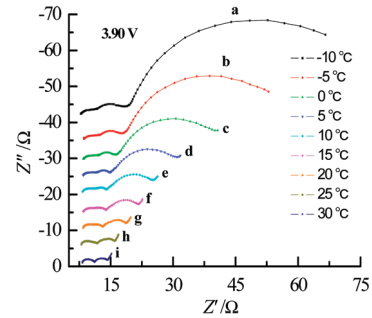

Figure 6. Nyquist plots of the spinel $LiMn_2O_4$ electrode at various temperatures at 3.90 V.

time constants.[26] Moreover, the same phenomenon could also be observed at a potential of 3.98 V (Figure 7). In view of the fact that most studies so far were carried out under room-temperature conditions (about 25 °C),[32−34] at intermediate intercalation degrees, there would be only two semicircles and one sloping line observed in the Nyquist plots, and not three

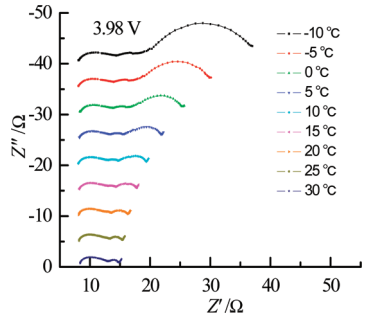

Figure 7. Nyquist plots of the spinel $LiMn_2O_4$ electrode at various temperatures at 3.98 V.

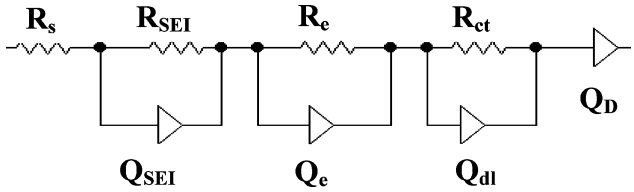

Figure 8. Equivalent circuit proposed for analysis of the spinel $LiMn_2O_4$ electrode in the first charge−discharge process.

semicircles as reported in the current paper. Therefore, the MHFS that appeared in our EIS spectra could be attributed to the effect of temperature.

As shown above, the high frequency compressed semicircle which was observed at room temperature by other authors[28−35] consisted of in fact two semicircles. Therefore, the semicircle in the high frequency region commonly observed in the Nyquist plots, which was attributed to lithium ion migration through the surface film by Aurbach et al.,[28,29,35] is not conclusive. Nobili et al.,[20,26,36−38] after investigation of the Li_xCoO_2 and other members of the family $Li_xNi_{1-y}Co_yO_2$ electrode by EIS, suggest that the effects of the finite electronic conductivity of the material should be clearly reflected in the Nyquist plots. Such a suggestion implies that three semicircles should be observed, although their papers did not show three conspicuous semicircles. As a result, the MHFS observed in this study may be assigned to the electronic properties of the material, which will be demonstrated below.

According to the experimental results obtained in this work, a new equivalent circuit, as shown in Figure 8, is proposed to fit the impedance spectra of the spinel $LiMn_2O_4$ electrode in the first charge−discharge process. In this equivalent circuit, R_s represents the ohmic resistance, and R_{SEI} and R_{ct} are resistances of the SEI film and the charge transfer reaction. The capacitance of the SEI film and the capacitance of the double layer are represented by the constant phase elements (CPE) Q_{SEI} and Q_{dl}, respectively. The low frequency region, however, cannot be modeled properly by a finite Warburg element. We have chosen, therefore, to replace the finite diffusion by a CPE, i.e., Q_D. This approach has been used to characterize the graphite electrode[39] and has allowed us to obtain a good agreement with the experimental data. The electronic resistance of the material and the associated capacitance used to characterize the electronic properties of the material are represented by R_e and the constant phase elements Q_e. The expression for the admittance response of the CPE (Q) is

$$Y = Y_0\omega^n \cos\left(\frac{n\pi}{2}\right) + jY_0\omega^n \sin\left(\frac{n\pi}{2}\right) \quad (1)$$

where ω is the angular frequency and j is the imaginary unit. A CPE represents a resistor when $n = 0$, a capacitor with capacitance of C when $n = 1$, an inductor when $n = -1$, and a Warburg resistance when $n = 0.5$.

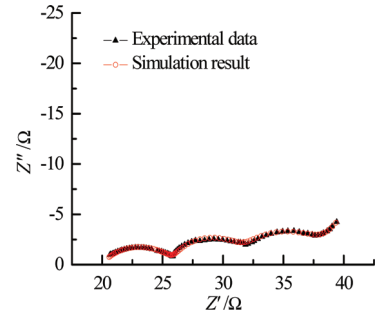

Figure 9. Comparison of EIS experimental data at 3.90 V in the first charge process with simulation results using the equivalent circuit of Figure 8.

TABLE 1: Equivalent Circuit Parameters Obtained from Fitting the Experimental Impedance Spectra at 3.9 V in the First Charge Process

parameters	valves	uncertainty (%)
R_{SEI}	6.523	1.8785
$Q_{SEI} - Y_0$	0.00024639	11.142
$Q_{SEI} - n$	0.65526	1.9253
R_e	10.224	3.8493
$Q_e - Y_0$	0.0066259	6.049
$Q_e - n$	0.87863	2.1435
R_{ct}	7.106	9.8172
$Q_{dl} - Y_0$	0.15335	7.5064
$Q_{dl} - n$	0.8821	4.183
$Q_D - Y_0$	1.539	23.908
$Q_D - n$	0.70312	9.0572

Figure 9 shows the simulated impedance spectra compared with experimental EIS data at 3.90 V in the charge process, and the values of the parameters are listed in Table 1. The relative standard deviations for most parameters obtained from fitting the experimental impedance spectra are within 15%, which demonstrated that the proposed model describes the experimental data satisfactorily.

Figure 10 illustrates variations of R_{SEI} with electrode potential obtained from fitting the experimental impedance spectra of the spinel $LiMn_2O_4$ electrode during the first charge−discharge cycle. As can be seen, R_{SEI} keeps almost constant below 3.75 V and above 4 V in the first charge−discharge process, which is similar to the data reported for the cycled $LiNiO_2$ electrode,[40] indicating that the SEI film remains persistent and stable to a certain extent in these processes. However, R_{SEI} increases and decreases reversibly in the potential region from 4 to 3.75 V. This may be due to the reversible breakdown (or dissolution) of the resistive SEI film, as proposed by Zhang et al.[41]

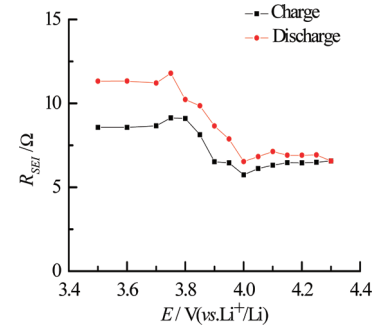

Figure 10. Variations of R_{SEI} with electrode potential obtained from fitting the experimental impedance spectra of the spinel $LiMn_2O_4$ electrode during the first charge−discharge cycle.

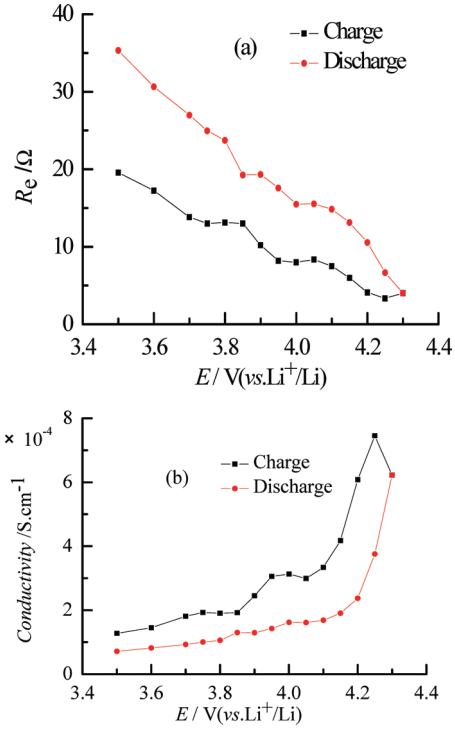

Figure 11. Variations of R_e (a) and the conductivity (b) derived from R_e with electrode potential obtained from fitting the experimental impedance spectra of the spinel $LiMn_2O_4$ electrode during the first charge−discharge cycle.

Among the characteristics of insertion materials, the electrical conductivity of the component materials is one of the most important issues in connection with the rate performance of batteries. In addition to such practical importance, conductivity measurements during the lithium insertion (and extraction) reaction would be an attractive approach for the study of the variation in the electronic structure of the materials as a function of lithium content.[42,43] Variations of R_e obtained from fitting the experimental impedance spectra of the spinel $LiMn_2O_4$ electrode and the conductivity derived from R_e with electrode potential during the first charge−discharge cycle are shown in Figure 11. The electronic resistance of the material in the charge and discharge process has the same trend of variation with potential; i.e., R_e decreases with the increase of electrode polarization potential in the charge process and increases with the decrease of electrode polarization potential in the discharge process. The conductivity derived from R_e is in the range of 10^{-4} S·cm^{-1}, being roughly in agreement with previous reports,[44,45] and exhibits a similar behavior to R_e varying with electrode polarization potential during the course of lithium extraction (and reinsertion) in $LiMn_2O_4$ in accordance with the results obtained by Nishizawa et al.[46] This demonstrated that the semicircle in the middle to high frequency region observed in this study should be assigned to the electronic properties of the material undoubtedly. Spinel $Li_{1-x}Mn_2O_4$ is a mixed-valence (Mn^{3+}/Mn^{4+}) compound, and its electronic conduction takes place by electron hopping between high-valence (Mn^{4+}) and low-valence (Mn^{3+}) cations.[47,48] Conductivity of this type would be governed by the concentration of carriers (electrons from Mn^{3+}) and the hopping length (Mn−Mn interatomic distance). The number of electron carriers decreases proportionally with the degree of delithiation coupled with oxidation of Mn^{3+} to Mn^{4+}. On the other hand, the Mn−Mn distance in the spinel structure is reduced by delithiation. The R_e change may result from the sum of these opposite effects, and it decreases with

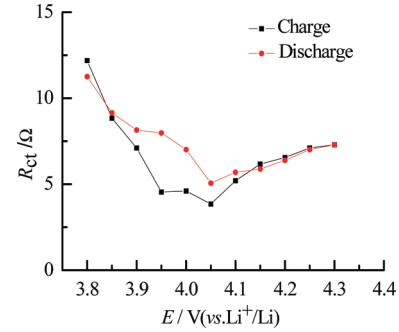

Figure 12. Variations of R_{ct} with electrode potential obtained from fitting the experimental impedance spectra of the spinel $LiMn_2O_4$ electrode during the first charge−discharge cycle.

an increase of the electrode polarization potential in the charge process, indicating that the effect of the contraction of hopping length predominated over the decrease of the numbers of electron carriers.

The R_{ct} versus E plot is supposed to behave according to the following classical equation[49]

$$R_{ct} = 1/fFk_0Ac_O^{0.5}c_R^{0.5} \quad (2)$$

In this equation, f denotes the usual electrochemical constant (equal to F/RT with F and R being the Faraday and gas constant, respectively, and T the absolute temperature), and k_0 is the heterogeneous rate constant. It should be noted that using eq 2 the total concentration of available intercalation sites, c_T, is constant, i.e., $c_O + c_R = c_T$. The concentration of the reduced form, c_R, and that of the oxidized form, c_O, are identified with the concentration of lithium ions and unoccupied intercalation sites, respectively. Equation 2 clearly predicts a rapid increase in R_{ct} as $c_O \rightarrow c_T$ or $c_R \rightarrow c_T$, i.e., for either the completely intercalated or deintercalated states. It can be observed from Figure 12 that R_{ct} is high at the low and high potentials and minimal at middle potentials in the charge process, and similar behavior can be also observed in the discharge process. The results confirmed that eq 2 can be used to correctly interpret the experimental data. As a consequence, the semicircle in the middle frequency is undoubtedly attributed to the charge-transfer process.

4. Physical Mechanism of Lithium Insertion and Deinsertion

Over the past 10 years, several models have been proposed to explain the impedance response of the insertion materials for lithium ion batteries, including anode materials such as graphite and cathode materials such as $LiMn_2O_4$, $LiMnO_2$, $LiNiO_2$, and $LiCoO_2$. Among these models, the modified Voigt−FMG equivalent circuit, suggested by Aurbach et al.,[29] is considered to provide the best account of the lithium ion insertion process in these insertion/deinsertion materials. This model reflects the steps involved during lithium ion insertion: diffusion of lithium ions in solution, lithium ion migration through the solid electrolyte interphase film, charge-transfer through the electrode/electrolyte interface, and solid state transport of lithium ions in the material matrix including solid state diffusion of lithium ions in the solid phase and occupation of lithium ions in the lattice. However, in the above model, the electrode is assumed to be built up of spherical particles of uniform size, and no change of the particle structure or new phase formation was taken into account. Barsoukov et al.,[12,50]

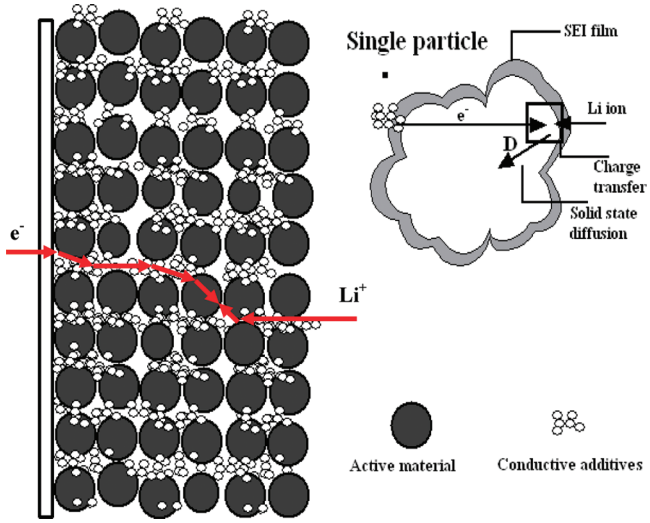

Figure 13. Pictorial representation model for lithium ion insertion/desertion into the intercalation electrode.

after characterizing lithium ion intercalation into and out of single carbon particles, proposed a new model. They supposed that the electrochemical kinetics characteristic of battery materials is represented by several common steps: (i) ionic charge conduction through electrolyte in the pores of the active layer and electronic charge conduction through the conductive part of the active layer; (ii) Lithium ion diffusion through the surface insulating layer of the active material; (iii) lithium ion diffusion in the solid phase; and (iv) a capacitive behavior that is related to the occupation of lithium ions and phase-transfer in cases where several phases are present. However, the effect of the conductive material during the lithium ion insertion/deinsertion process was underestimated by Barsoukov et al.[12,50]

As noted above, the lithium ions flow through the electrolyte, whereas the electrons are generated from the reaction, $Li = Li^+ + e^-$, and go through the external circuit to do work. Thus, the electrode system must allow for the flow of both lithium ions and electrons. That is, it must be both a good ionic and electronic conductor. It is well-known that many electrochemically active materials are not good electronic conductors. Consequently, it is necessary to add an electronically conductive material such as carbon black. To physically hold the electrode together, a binder is also added. In these cases, the electrochemical reaction can only occur at those points where they meet the active material, the conductive diluent and electrolyte meet.[51] So the electrical conductivity of the component materials is one of the most important issues in connection with the performance of batteries. In this paper, a modified model (Figure 13) is put forward, based on the experimental results above, to explain the impedance response of the insertion materials of lithium ion batteries. As can be seen from Figure 13, because the surface film (SEI film) caused by the reaction between the oxide and electrolyte is ionically conducting but electronically insulating,[52] it is possible that electron charge conduction through or out of the particles takes place as follows: (a) the electrons are transported to the points where they meet the active material and the conductive material and (b) the electrons then diffuse inside the active particles. As analyzed above, it is reasonable that the EIS spectra are interpreted in terms of the following physical phenomena in an order of decreasing frequency: (1) a high frequency dispersion because of the presence of a surface layer, (2) a middle to high frequency dispersion related to the electronic properties of the material, (3) a middle frequency semicircle associated with charge transfer, and finally, (4) the very low frequency dispersion attributed to the solid state diffusion. We propose to assign the middle to high frequency semicircle to the electronic resistance of the material and the middle frequency semicircle to the charge-transfer process, based on the following reasons: (1) the variations of the parameters (R_e and R_{ct}) obtained from the equivalent circuit in the third part of the present paper, and (2) following the adatom model, as adapted by Bruce and Saidi,[53] the process is accompanied by the insertion of an electron into the conduction band of the host, followed by diffusion of Li ions to the intercalation site, where it becomes fully incorporated into the lattice. Therefore, the charge-transfer process must come after the electron transport.

5. Conclusions

The first delithiation−lithiation process of spinel $LiMn_2O_4$ at different potentials and different temperatures has been investigated by electrochemical impedance spectroscopy. It has revealed that, at intermediate degrees of intercalation, three semicircles appear in the Nyquist diagram. The three semicircles have been assigned to the Li ion migration through the surface film, the electronic properties of the material, and a charge-transfer step, respectively. On the basis of the experimental results, a modified model has been put forward to explain successfully the impedance response of the insertion materials for lithium ion batteries.

Acknowledgment. The authors thank the National Basic Research Program of China (No. 2009CB220102) for financial support.

References and Notes

(1) Winter, M.; Besenhard, J. O.; Spahr, M. E.; Novák, P. *Adv. Mater.* **1998**, *10*, 725.
(2) Ogumi, Z.; Inaba, M. *Bull. Chem. Soc. Jpn.* **1998**, *71*, 521.
(3) Armstrong, A. R.; Bruce, P. G. *Nature.* **1996**, *381*, 499.
(4) Broussely, M.; Biensan, P.; Simon, B. *Electrochim. Acta* **1999**, *45*, 3.
(5) Park, H. S.; Hwang, S. J.; Choy, J. H. *J. Phys. Chem. B* **2001**, *105*, 4860.
(6) Kovacheva, D.; Gadjov, H.; Petrov, K.; Mandal, S.; Lazarraga, M. G.; Pascual, L.; Amarilla, J. M.; Rojas, R. M.; Herrero, P.; Rojo, J. M. *J. Mater. Chem.* **2002**, *12*, 1184.
(7) Whittingham, M. S. *Chem. Rev.* **2004**, *104*, 4271.
(8) Yu, L. H.; Yang, H. X.; Ai, X. P.; Cao, Y. L. *J. Phys. Chem. B* **2005**, *109*, 1148.
(9) Wang, Y.; Takahashi, K.; Shang, H. M.; Cao, G. Z. *J. Phys. Chem. B* **2005**, *109*, 3085.
(10) Jiao, F.; Shaju, K. M.; Bruce, P. G. *Angew. Chem., Int. Ed.* **2005**, *44*, 6550.
(11) Arico, A. S.; Bruce, P. G.; Scrosati, B.; Tarascon, J. M.; Schalkwijk, V. *Nat. Mater.* **2005**, *4*, 366.
(12) Barsoukov, E.; Kim, D. H.; Lee, H.-S.; Lee, H.; Yakovleva, M.; Gao, Y.; Engel, J. F. *Solid State Ionics* **2003**, *161*, 19.
(13) Kazakopoulos, A.; Sarafidis, C.; Chrissafis, K.; Kalogirou, O. *Solid State Ionics* **2008**, *179*, 1980.
(14) Levi, M. D.; Aurbach, D. *J. Phys. Chem. C* **2005**, *109*, 2763.
(15) Doia, T.; Yahiro, T.; Okada, S.; Yamaki, J. *Electrochim. Acta* **2008**, *53*, 8064.
(16) Aurbach, D.; Levi, M. D.; Levi, E. *Solid State Ionics* **2008**, *179*, 742.
(17) Itagaki, M.; Kobari, N.; Yotsuda, S.; Watanabe, K.; Kinoshita, S.; Ue, M. *J. Power Sources* **2005**, *148*, 78.
(18) Dokko, K.; Mohamedi, M.; Umeda, M.; Uchida, I. *J. Electrochem. Soc.* **2003**, *150*, A425.
(19) Kobayashi, S.; Uchimoto, Y. *J. Phys. Chem. B* **2005**, *109*, 13322.
(20) Croce, F.; Nobili, F.; Deptula, A.; Lada, W.; Tossici, R.; D'Epifanio, A.; Scrosati, B.; Marassi, R. *Electrochem. Commun.* **1999**, *1*, 605.
(21) Morita, M.; Yamada, O.; Ishikawa, M. *J. Power Sources* **1999**, *81*−*82*, 425.
(22) Hjelm, A.-K.; Lindbergh, G. *Electrochim. Acta* **2002**, *47*, 1747.

(23) Mohamedi, M.; Takahashi, D.; Itoh, T.; Umeda, M.; Uchida, I. *J. Electrochem. Soc.* **2002**, *149*, A19.
(24) Striebel, K. A.; Sakai, E.; Cairns, E. J. *J. Electrochem. Soc.* **2002**, *149*, A61.
(25) Dokko, K.; Mohamedi, M.; Umeda, M.; Uchida, I. *J. Electrochem. Soc.* **2003**, *150*, A425.
(26) Nobili, F.; Tossici, R.; Marassi, R.; Croce, F.; Scrosati, B. *J. Phys. Chem. B* **2002**, *106*, 3909.
(27) Nakayama, M.; Ikuta, H.; Uchimoto, Y.; Wakihara, M. *J. Phys. Chem. B* **2003**, *107*, 10603.
(28) Aurbach, D.; Levi, M. D.; Levi, E.; Telier, H.; Markovsky, B.; Salitra, G.; Heider, U.; Hekier, L. *J. Electrochem. Soc.* **1998**, *145*, 3024.
(29) Aurbach, D.; Gamolsky, K.; Markovsky, B.; Salitra, G.; Gofer, Y.; Heider, U.; Oesten, R.; Schmidt, M. *J. Electrochem. Soc.* **2000**, *147*, 1322.
(30) Johnson, B. J.; Doughty, D. H.; Voigt, J. A.; Boyle, T. J. *J. Power Sources* **1997**, *68*, 634.
(31) Barker, J.; West, K.; Saidi, Y.; Pynenburg, R.; Zachau-Christiansen, B.; Koksbang, R. *J. Power Sources* **1995**, *54*, 475.
(32) Lu, D.; Li, W.; Zuo, X.; Yuan, Z.; Huang, Q. *J. Phys. Chem. C* **2007**, *111*, 12067.
(33) Tu, J.; Zhao, X. B.; Cao, G. S.; Tu, J. P.; Zhu, T. J. *Mater. Lett.* **2006**, *60*, 3251–3254.
(34) Yamada, O.; Ishikawa, M.; Morita, M. *Electrochim. Acta* **2000**, *45*, 2197.
(35) Aurbach, D.; Levi, M. D.; Gamulski, K.; Markovsky, B.; Salitra, G.; Levi, E.; Heider, U.; Heider, L.; Oesten, R. *J. Power Sources* **1999**, *81*−*82*, 472.
(36) Nobili, F.; Dsoke, S.; Minicucci, M.; Croce, F.; Marassi, R. *J. Phys. Chem. B* **2006**, *110*, 11310.
(37) Nobili, F.; Tossici, R.; Croce, F.; Scrosati, B.; Marassi, R. *J. Power Sources* **2000**, *98*, 238.
(38) Nobili, F.; Croce, F.; Scrosati, B.; Marassi, R. *Chem. Mater.* **2001**, *13*, 1642.
(39) Zhang, S.; Shi, P. *Electrochim. Acta* **2004**, *49*, 1475.
(40) Aurbach, D.; Gamolsky, K.; Markovsky, B.; Salitra, G.; Gofer, Y.; Heider, U.; Oesten, R.; Schmidt, M. *J. Electrochem. Soc.* **2000**, *147*, 1322.
(41) Zhang, S. S.; Xu, K.; Jow, T. R. *J. Electrochem. Soc.* **2002**, *149*, A1521.
(42) Molenda, J. *Solid State Ionics* **2004**, *175*, 203.
(43) Molenda, J. *Solid State Ionics* **2005**, *176*, 1687.
(44) Kanoh, H.; Feng, Q.; Hirotsu, T.; Ooi, K. *J. Electrochem. Soc.* **1996**, *143*, 2610.
(45) Molenda, J.; Swierczek, K.; Kucza, W.; Marzec, J.; Stoklosa, A. *Solid State Ionics* **1999**, *123*, 155.
(46) Nishizawa, M.; Ise, T.; Koshika, H.; Itoh, T.; Uchida, I. *Chem. Mater.* **2000**, *12*, 1367.
(47) Pistoia, G.; Zane, D.; Zhang, Y. *J. Electrochem. Soc.* **1995**, *142* (8), 2551–2557.
(48) Marzec, J.; Świerczek, K.; Przewoźnik, J.; Molenda, J.; R Simon, D.; M Kelder, E.; Schoonman, J. *Solid State Ionics.* **2002**, *146*, 225–237.
(49) Levi, M. D.; Gamolsky, K.; Aurbach, D.; Heide, U.; Oesten, R. *Electrochim. Acta* **2000**, *45*, 1781.
(50) Barsoukov, E.; Kim, J. H.; Kim, J. H.; Yoon, C. O.; Lee, H. *Solid State Ionics* **1999**, *116*, 249.
(51) Whittingham, M. S. *Chem. Rev.* **2004**, *104*, 4271.
(52) Hjelm, A.-K.; Lindbergh, G. *Electrochim. Acta* **2002**, *47*, 1747.
(53) Bruce, P. G.; Saidi, M. Y. *J. Electroanal. Chem.* **1992**, *322*, 93.

JP9109157